Last time | Mueller's Dipole Model and Nonlinear Small-x Evolution (cont'd)

Need $\alpha_s \ln \frac{1}{x}$ corrections to the GGM f-la:

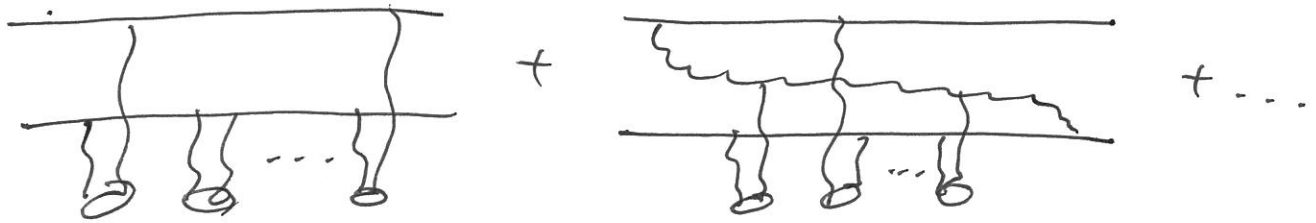

To find one-gluon correction, need LC wave function

$$= i \frac{g t^a}{\pi} \underline{\varepsilon}^*_\lambda \cdot \left(\frac{\underline{x}_{21}}{x_{12}^2} - \frac{\underline{x}_{20}}{x_{20}^2} \right)$$

element in the square brackets of Eq. (4.56) simplify to

$$\bar{u}_\sigma(k_1)\gamma\cdot\epsilon^*_\lambda(k_2)u_{\sigma''}(k_1+k_2)\approx\frac{1}{2}\bar{u}_\sigma(k_1)\gamma^+u_{\sigma''}(k_1+k_2)\epsilon^-_\lambda(k_2)^*$$
$$=2\delta_{\sigma\sigma''}\sqrt{k_1^+(k_1^++k_2^+)}\,\frac{\vec{\epsilon}^{\,\lambda*}_\perp\cdot\vec{k}_{2\perp}}{k_2^+}\approx 2\delta_{\sigma\sigma''}k_1^+\frac{\vec{\epsilon}^{\,\lambda*}_\perp\cdot\vec{k}_{2\perp}}{k_2^+}. \tag{4.58}$$

Performing a similar approximation for the second matrix element in Eq. (4.56) and inserting the result along with Eqs. (4.57) and (4.58) back into Eq. (4.56) yields

$$\Psi^{(1)}_{\sigma\sigma'}(\vec{k}_{1\perp},\vec{k}_{2\perp},z_1,z_2)$$
$$\approx 2gt^a\theta(z_2)\frac{\vec{\epsilon}^{\,\lambda*}_\perp\cdot\vec{k}_{2\perp}}{k^2_{2\perp}}\left[\Psi^{(0)}_{\sigma\sigma'}(\vec{k}_{1\perp}+\vec{k}_{2\perp},z_1)-\Psi^{(0)}_{\sigma\sigma'}(\vec{k}_{1\perp},z_1)\right], \tag{4.59}$$

where we have also neglected z_2 in comparison with z_1 in the argument of one wave function.

In the transverse coordinate space representation, Eq. (4.59) has the form

$$\Psi^{(1)}_{\sigma\sigma'}(\vec{x}_{10},\vec{x}_{20},z_1,z_2)=\int\frac{d^2k_{1\perp}d^2k_{2\perp}}{(2\pi)^4}e^{i\vec{k}_{1\perp}\cdot\vec{x}_{10}+i\vec{k}_{2\perp}\cdot\vec{x}_{20}}\Psi^{(1)}_{\sigma\sigma'}(\vec{k}_{1\perp},\vec{k}_{2\perp},z_1,z_2)$$
$$=i\frac{gt^a}{\pi}\Psi^{(0)}_{\sigma\sigma'}(\vec{x}_{10},z_1)\,\vec{\epsilon}^{\,\lambda*}_\perp\cdot\left(\frac{\vec{x}_{21}}{x^2_{21}}-\frac{\vec{x}_{20}}{x^2_{20}}\right), \tag{4.60}$$

where $\vec{x}_{20}=\vec{x}_{2\perp}-\vec{x}_{0\perp}$, $\vec{x}_{21}=\vec{x}_{2\perp}-\vec{x}_{1\perp}$, and $x_{ij}=|\vec{x}_{ij}|$ as defined after Eq. (1.87). The gluon has transverse coordinate $\vec{x}_{2\perp}$, as illustrated in Fig. 4.13. We have used Eq. (A.10) to obtain Eq. (4.60) from Eq. (4.59).

Squaring the coordinate-space one-gluon wave function from Eq. (4.60) and summing over the quark and gluon polarizations and colors yields

$$\sum_{\sigma,\sigma',\lambda,a}\left|\Psi^{(1)}_{\sigma\sigma'}\right|^2=\frac{4\alpha_sC_F}{\pi}\frac{x^2_{10}}{x^2_{20}x^2_{21}}\sum_{\sigma,\sigma'}\left|\Psi^{(0)}_{\sigma\sigma'}\right|^2. \tag{4.61}$$

To calculate the probability of finding one extra gluon in the onium wave function we have to integrate Eq. (4.61) over the gluon's phase space, which, in the $z_2\ll z_1$, $1-z_1\ll 1$ approximation, is (cf. Eq. (4.23))[4]

$$\int_{z_0}^{\min\{z_1,1-z_1\}}\frac{dz_2}{z_2}\int\frac{d^2x_2}{4\pi}, \tag{4.62}$$

where z_0 is some lower cutoff on the z_2-integral, imposed to make the integration finite; the exact value of z_0 depends on the physical process corresponding to the wave function we are constructing. The order-α_s contribution to the probability of finding one gluon inthe

[4] One may ask why, if our calculation is valid for $z_2\ll z_1$, $1-z_1$, we can extend the z_2-integral all the way up to z_1 or $1-z_1$. While indeed our approximation breaks down for z_2 close to z_1 or $1-z_1$, putting z_1 or $1-z_1$ as the upper integration limit gives the correct leading-logarithmic contribution.

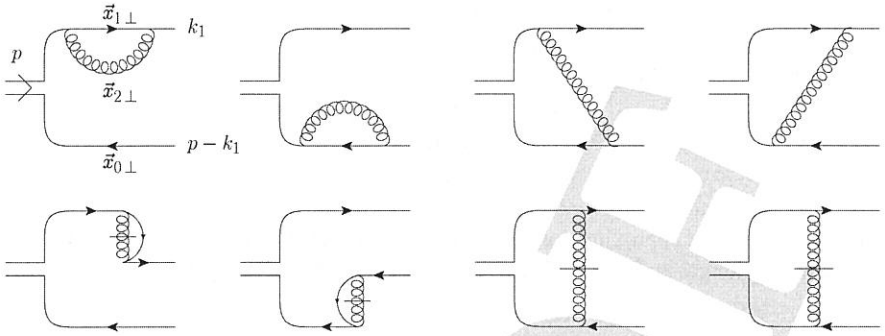

Fig. 4.14. Virtual contribution to small-x evolution in the onium wave function. The quark transverse coordinates in the onium are not changed by the corrections.

onium wave function is then (Mueller 1994)

$$\int_{z_0}^{\min\{z_1,1-z_1\}} \frac{dz_2}{z_2} \int \frac{d^2x_2}{4\pi} \sum_{\sigma,\sigma',\lambda,a} \left|\Psi^{(1)}_{\sigma\sigma'}\right|^2 = \int_{z_0}^{\min\{z_1,1-z_1\}} \frac{dz_2}{z_2} \int d^2x_2 \frac{\alpha_s C_F}{\pi^2} \frac{x_{10}^2}{x_{20}^2 x_{21}^2} \sum_{\sigma,\sigma'} \left|\Psi^{(0)}_{\sigma\sigma'}\right|^2 . \tag{4.63}$$

Note that the modified wave function in Eq. (4.63) contains a power of α_s and a logarithmic integral over z_2, which would give us finally $\ln 1/x$. We see that the modification we have calculated brings in a factor $\alpha_s \ln 1/x$. Another feature of Eq. (4.63) is that the $\vec{x}_{2\perp}$-integral in it contains UV divergences at $x_{20} \approx 0$ and $x_{21} \approx 0$. For now we will regulate these divergences by a UV cutoff ρ, such that $x_{20}, x_{21} > \rho$: in the end no physical quantity depends on the value of this cutoff.

Before we proceed let us point out that, as for the Glauber–Gribov–Mueller model (see e.g. Eq. (4.41)), the expression (4.63) completely factorizes transverse coordinate space into the square of the "bare" onium wave function times the probability of emission of the extra gluon. The emission of an extra gluon does not change the coordinates of the initial quark and the antiquark, yet again illustrating our above argument about the convenience of the transverse coordinate representation. This property also gives Eq. (4.61) a very simple physical meaning, resulting from the probabilistic interpretation of the light cone wave functions: the contribution to the onium wave function due to the emission of an extra gluon is equal to the product of the probability of finding a dipole with size x_{10} inside the onium ($\sim |\Psi^{(0)}_{\sigma\sigma'}|^2$) multiplied by the probability that the dipole emits a gluon at $\vec{x}_{2\perp}$.

The one-gluon corrections to the dipole wave function need not be limited to the "real" gluon shown in Fig. 4.13; they should also include virtual corrections, where the gluon is both emitted and absorbed in the onium wave function, again like in the DGLAP case in Sec. 2.4.2. The virtual diagrams giving the LLA contributions are shown in Fig. 4.14, where, in accordance with the LCPT rules introduced in Sec. 1.3, the crossed lines denote instantaneous terms. From the sheer number of graphs in Fig. 4.14 one can see that direct calculation of all the virtual corrections can be a daunting task (see Chen and Mueller

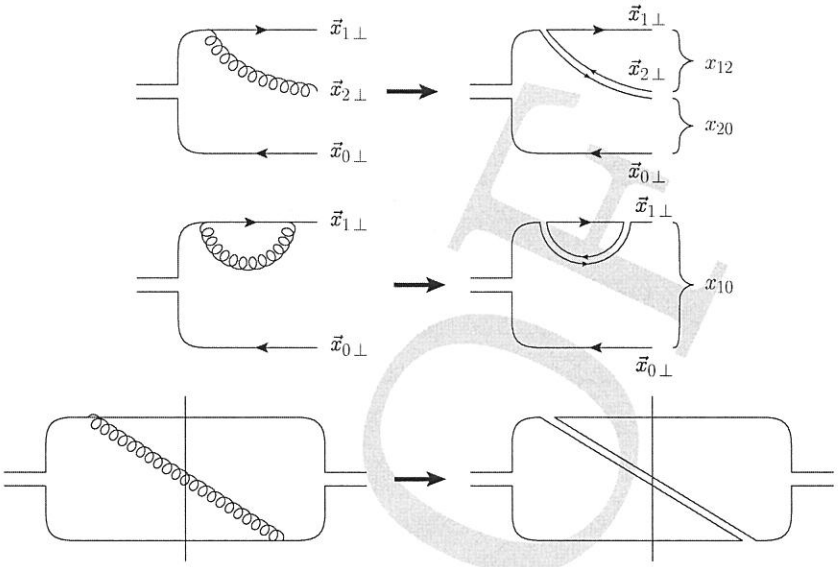

Fig. 4.15. Large-N_c limit in the onium wave function (top two panels) and the wave function squared (bottom panel). The curly brackets in the top panel denote the daughter dipoles generated by the gluon emission. The right-hand brace in the middle panel denotes the parent dipole remaining intact after a virtual correction. The thin vertical line in the bottom panel separates the wave function from its complex conjugate.

(1995) for an outline of the calculation). Instead we will follow Mueller (1994) and use the unitarity argument presented in Sec. 2.4.2 (see Eq. (2.86)) to write down the following expression for the order-α_s virtual correction to the onium wave function:

$$\Psi^{(0)}_{\sigma\sigma'}(\vec{x}_{10}, z_1)\Big|_{O(\alpha_s)} = -\frac{1}{2}\int\limits_{z_0}^{\min\{z_1,1-z_1\}} \frac{dz_2}{z_2}\int d^2x_2 \frac{\alpha_s C_F}{\pi^2}\frac{x_{10}^2}{x_{20}^2 x_{21}^2}\,\Psi^{(0)}_{\sigma\sigma'}(\vec{x}_{10}, z_1)\Big|_{O(\alpha_s^0)}$$

$$= -\frac{2\alpha_s C_F}{\pi}\ln\frac{x_{01}}{\rho}\int\limits_{z_0}^{\min\{z_1,1-z_1\}} \frac{dz_2}{z_2}\,\Psi^{(0)}_{\sigma\sigma'}(\vec{x}_{10}, z_1)\Big|_{O(\alpha_s^0)}. \qquad (4.64)$$

The integral over $\vec{x}_{2\perp}$ is carried out in appendix section A.3 with ρ the UV regulator introduced above.

Having obtained the one-gluon corrections we would now like to derive an equation resumming the higher-order gluon emissions and virtual gluon corrections that bring powers of $\alpha_s \ln 1/x$ into the wave function. (Remember that quark loops do not contribute leading logarithms of x.) This turns out to be a rather difficult problem. A major simplification occurs if we consider the onium wave function in the 't Hooft large-N_c limit ('t Hooft 1974), taking N_c to be very large while keeping $\alpha_s N_c$ constant. In the large-N_c limit the single gluon line is replaced by a double line, corresponding to replacing the gluon by a quark–antiquark pair in the color-octet configuration. This is illustrated in Fig. 4.15. In the

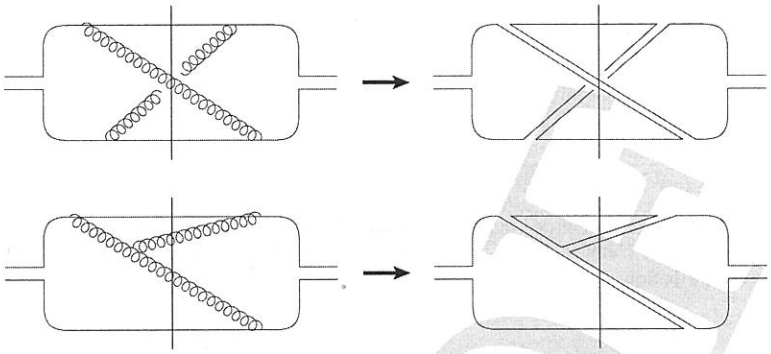

Fig. 4.16. Two steps of small-x evolution in the onium wave function squared (left) and their large-N_c limits (right). The top panel shows a nonplanar diagram, which is N_c^2-suppressed compared with the leading-N_c planar diagram shown in the bottom panel.

large-N_c limit it is convenient to talk about color dipoles instead of gluons. The original onium is a color dipole consisting of a quark at $\vec{x}_{1\perp}$ and an antiquark at $\vec{x}_{0\perp}$. The emission of a gluon in the onium wave function, taken in the large-N_c limit, corresponds to the splitting of the original dipole with size x_{10} into two dipoles with sizes x_{12} and x_{20}: the dipole the size x_{12} consists of the original quark at $\vec{x}_{1\perp}$ and the antiquark part of the gluon line at $\vec{x}_{2\perp}$, while the quark part of the gluon line at $\vec{x}_{2\perp}$ along with the original antiquark at $\vec{x}_{0\perp}$ form the dipole with size x_{20} (see the top and bottom panels of Fig. 4.15). The virtual gluon corrections leave the original dipole intact, as can be seen in the middle panel of Fig. 4.15.

Another important feature of the large-N_c limit is that only *planar diagrams* contribute; the nonplanar diagrams are suppressed by powers of N_c for fixed $\alpha_s N_c$. This means that different color dipoles generated by gluon emissions do not "talk" to each other: subsequent emissions happen independently in each dipole. This is illustrated in Fig. 4.16, where in the top panel we show an example of a diagram where a gluon emitted in one dipole in the amplitude connects to another dipole in the complex conjugate amplitude. As can be seen from Fig. 4.16, such diagram is indeed nonplanar; hence, it is $1/N_c^2$-suppressed (as can be checked explicitly) and can be neglected in the large-N_c limit. At the same time, the diagram in the lower panel of Fig. 4.16, while of the same order in $\alpha_s \ln 1/x$, is also planar: in it the gluon from one dipole does not interact with the other dipole, remaining instead in its own dipole. This second diagram in Fig. 4.16 is of leading order in N_c and has to be resummed by large-N_c dipole evolution. (Strictly speaking, the diagram in the lower left panel of Fig. 4.16, when written in double-line notation, also contains a nonplanar subleading-N_c correction, in which the quark line in the longer gluon interacts with the quark of the original dipole: this correction is not shown in Fig. 4.16.)

Note that, in order to obtain the leading-$\ln 1/x$ contribution to the wave function, the softer gluons (those with smaller z) have to be emitted later (to the right in our LCPT diagrams) than the harder gluons, with larger values of z. For instance, consider an onium wave function with two gluon emissions, as shown in Fig. 4.17. Assume further that the gluon emitted earlier is softer than the gluon emitted later, i.e., that $z_3 \ll z_2$, where, as

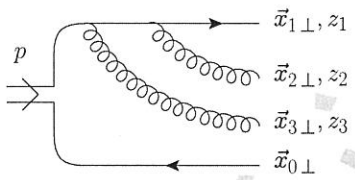

Fig. 4.17. Two gluons emitted in the onium wave function: if one assumes that the gluon emitted earlier is softer, $z_3 \ll z_2$, then the square of this diagram will not give a leading-$\ln 1/x$ contribution.

usual,

$$z_i = \frac{k_i^+}{p^+}. \tag{4.65}$$

A simple calculation of the wave function in Fig. 4.17, in the $z_3 \ll z_2$ approximation, carried out along the steps outlined above for a single emission would yield a wave function proportional to z_3/z_2 as far as the longitudinal momentum dependence is concerned. Squaring this wave function and integrating the result over z_2 and z_3 with $z_1 \gg z_2 \gg z_3 \gg z_0$ yields an answer proportional to

$$\alpha_s^2 \int_{z_0}^{z_1} \frac{dz_2}{z_2} \int_{z_0}^{z_2} \frac{dz_3}{z_3} \frac{z_3^2}{z_2^2} \approx \frac{1}{2} \alpha_s^2 \ln \frac{z_1}{z_0}. \tag{4.66}$$

We see that we have only one longitudinal logarithm per two powers of the coupling α_s: this is not a leading logarithmic contribution. Hence the square of the diagram in Fig. 4.17 is subleading in $\ln 1/x$ and does not contribute to the leading-$\ln 1/x$ evolution we are considering here. It does contribute when one attempts to calculate the NLO corrections to the evolution we are about to construct (see Chapter 6). Using similar arguments, one can show that the diagram in Fig. 4.17 does not contribute to the LLA, even when we take its overlap with the wave function resulting when gluon 3 is emitted after gluon 2. In fact one can also show that no diagram with inverse time-ordering like that in Fig. 4.17 contributes in the LLA approximation. We thus come to another important conclusion: to obtain LLA evolution in the wave function, the gluon emissions with

$$z_2 \gg z_3 \gg \cdots \gg z_n \tag{4.67}$$

must be ordered in time, with the harder (larger-z) gluons emitted *before* the softer (small-z) gluons.

Now the structure of the small-x light cone wave function becomes manifest: in one step of evolution a gluon is emitted. It can be a real gluon, like those in the top and bottom panels of Fig. 4.15, which would split the initial (parent) dipole 10 ("one-zero") into two new (daughter) dipoles 12 and 20. The subsequent $\alpha_s \ln 1/x$ evolution is driven by further gluon emission: this would happen independently (and in parallel) in both daughter dipoles. An example of two-gluon emission is shown in the second panel of Fig. 4.16. Alternatively, the emission in the initial dipole can be virtual, as shown in the middle panel of Fig. 4.15;

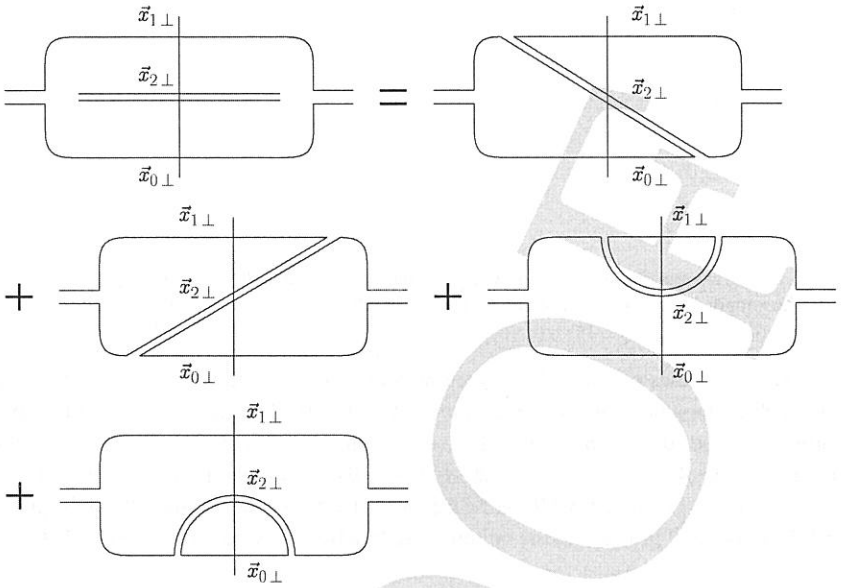

Fig. 4.18. Definition of an abbreviated notation for the sum of all large-N_c diagrams contributing to the real-gluon emission in the square of an onium wave function.

then the initial dipole remains intact, any subsequent evolution occurring within the initial dipole at later times.

As we can see from Eqs. (4.63) and (4.64), in the mixed representation in which we are working, each step of the evolution factorizes from the previous one, simplifying the construction of the gluon wave function. To illustrate this, let us consider two steps of small-x evolution due to two consecutive real-gluon emissions, including all possible LLA diagrams. It is convenient to introduce the shorthand diagram notation presented in Fig. 4.18, where the sum of all four (large-N_c) diagrams corresponding to real-gluon emission in the onium wave function comprises one diagram, that in the upper left of the figure. The diagrams in Fig. 4.18 give us the correction to the dipole wave function in Eq. (4.63). The kernel of this correction can be decomposed as follows:

$$\frac{\alpha_s C_F}{\pi^2} \frac{x_{10}^2}{x_{20}^2 x_{21}^2} = \frac{\alpha_s C_F}{\pi^2} \left(\frac{1}{x_{21}^2} - 2 \frac{\vec{x}_{21} \cdot \vec{x}_{20}}{x_{21}^2 x_{20}^2} + \frac{1}{x_{20}^2} \right), \tag{4.68}$$

where the first and the last terms on the right-hand side of Eq. (4.68) correspond to the last two graphs in Fig. 4.18, while the first two (interference) diagrams on the right of Fig. 4.18 give the second term on the right of Eq. (4.68). The very first diagram in Fig. 4.18 corresponds to the full emission kernel on the left of Eq. (4.68).

Using the notation of Fig. 4.18, the square of the large-N_c onium wave function with two real gluons in it in the LLA approximation can be represented simply by the two diagrams depicted in Fig. 4.19, with the gluons ordered in longitudinal momenta such that $z_2 \gg z_3$.

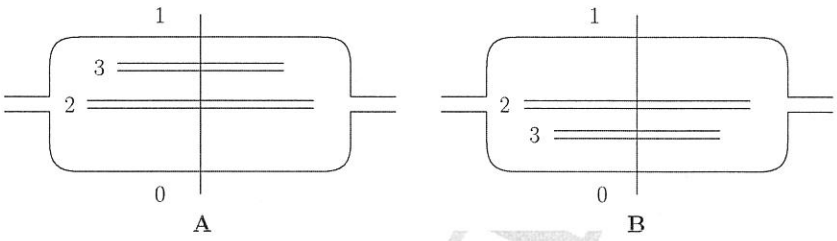

Fig. 4.19. Two real gluons in the LLA approximation and in the large-N_c limit contributing to the square of an onium wave function. The length of the lines is driven by light cone time-ordering.

According to the rules outlined above, the gluon carrying momentum fraction z_2 has to be emitted before the gluon carrying z_3, as shown in Fig. 4.19. The emission of gluon 2 splits the original dipole 10 into two dipoles. The subsequent emission of gluon 3 can occur either in dipole 12 (Fig. 4.19A) or in dipole 20 (Fig. 4.19B). (Note that gluon 3 is emitted from gluon 2 via a three-gluon vertex.) Iterating Eq. (4.63) twice, we see that the sum of the graphs A and B in Fig. 4.19 brings into the onium wave function squared the following factor:

$$\int\limits_{z_0}^{z_1} \frac{dz_2}{z_2} \int\limits_{z_0}^{z_2} \frac{dz_3}{z_3} \int d^2x_2 d^2x_3 \left(\frac{\alpha_s C_F}{\pi^2}\right)^2 \frac{x_{10}^2}{x_{20}^2 x_{21}^2} \left(\frac{x_{12}^2}{x_{31}^2 x_{32}^2} + \frac{x_{20}^2}{x_{32}^2 x_{30}^2}\right). \tag{4.69}$$

(For simplicity of notation we have put z_1 as the upper cutoff of the z_2-integration, since at LLA accuracy one cannot see any significant difference between z_1 and $1 - z_1$.) Equation (4.69) demonstrates that the small-x evolution in the onium wave function consists of consecutive emissions ordered in rapidity and light cone time, with the transverse dynamics included in a factorized way.

To describe the onium wave function formally including $\alpha_s \ln 1/x$ corrections to all orders it is convenient to define the *dipole generating functional* $Z(\vec{x}_{10}, \vec{b}_{0\perp}, Y; u)$ by

$$\begin{aligned} & Z(\vec{x}_{10}, \vec{b}_{0\perp}, Y; u) \sum_{\sigma\sigma'} |\Psi^{(0)}_{\sigma\sigma'}(\vec{x}_{10}, z_1)|^2 \Big|_{O(\alpha_s^0)} \\ &= \int d^2r_1 d^2b_1 |\Psi^{[1]}(\vec{r}_{1\perp}, \vec{b}_{1\perp}, Y)|^2 u(\vec{r}_{1\perp}, \vec{b}_{1\perp}) \\ &\quad + \frac{1}{2!} \int d^2r_1 d^2b_1 d^2r_2 d^2b_2 |\Psi^{[2]}(\vec{r}_{1\perp}, \vec{b}_{1\perp}, \vec{r}_{2\perp}, \vec{b}_{2\perp}, Y)|^2 \\ &\qquad \times u(\vec{r}_{1\perp}, \vec{b}_{1\perp}) u(\vec{r}_{2\perp}, \vec{b}_{2\perp}) + \cdots \\ &= \sum_{n=1}^{\infty} \frac{1}{n!} \int d^2r_1 d^2b_1 \cdots d^2r_n d^2b_n |\Psi^{[n]}(\vec{r}_{1\perp}, \vec{b}_{1\perp}, \ldots, \vec{r}_{n\perp}, \vec{b}_{n\perp}, Y)|^2 \\ &\qquad \times u(\vec{r}_{1\perp}, \vec{b}_{1\perp}) \cdots u(\vec{r}_{n\perp}, \vec{b}_{n\perp}). \end{aligned} \tag{4.70}$$

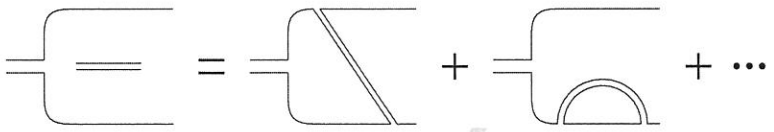

Fig. 4.20. An abbreviated notation for the sum of all large-N_c diagrams contributing to the virtual gluon correction to the onium wave function.

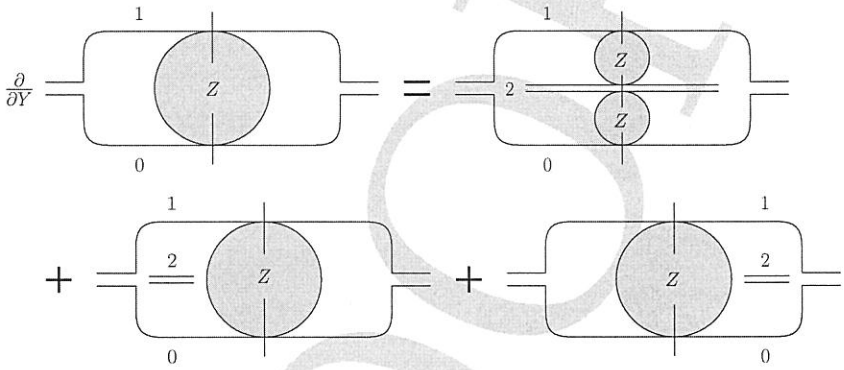

Fig. 4.21. Diagrammatic representation for the evolution equation of the generating functional Z (denoted by a shaded circle).

$|\Psi^{[n>1]}(Y=0)|^2 = 0$ and

$$|\Psi^{[1]}(\vec{r}_{1\perp}, \vec{b}_{1\perp}, Y=0)|^2 = \delta^2\left(\vec{b}_{1\perp} + \frac{\vec{r}_{1\perp}}{2} - \vec{x}_{1\perp}\right)\delta^2\left(\vec{b}_{1\perp} - \frac{\vec{r}_{1\perp}}{2} - \vec{x}_{0\perp}\right), \tag{4.75}$$

such that

$$Z(\vec{x}_{10}, \vec{b}_{0\perp}, Y=0; u) = u(\vec{x}_{10}, \vec{b}_{0\perp}). \tag{4.76}$$

Now that we have the initial conditions for Z-evolution, it is straightforward to write down an evolution equation for Z. The main principle was stated several pages ago: in one step of evolution a gluon is emitted in the dipole wave function: the gluon may be real, splitting the parent dipole into two daughter dipoles, or it may be virtual, leaving the parent dipole intact. In the former case the subsequent evolution continues independently in the two daughter dipoles, while in the latter case evolution continues in the parent dipole. This statement is illustrated diagrammatically in Fig. 4.21, where the generating functional Z is represented by a shaded circle. The first graph on the right of Fig. 4.21 corresponds to real-gluon emission, while the remaining two graphs represent the sum of all virtual corrections, as shown in Fig. 4.20.

Guided by Fig. 4.21, and employing Eqs. (4.63) and (4.64) while replacing C_F by $N_c/2$ in the large-N_c limit, we can write down the following evolution equation for the generating

so that

$$\ln^2 \left| \frac{\rho_{11'}\rho_{00'}}{\rho_{10'}\rho_{01'}} \right| = \ln^2 |1 - w|. \tag{4.128}$$

4.4 The Balitsky–Kovchegov equation

We now return to the DIS process in the dipole picture of Sec. 4.1. As follows from Eqs. (4.12) and (4.24), in order to find the DIS structure function all one needs is to find the imaginary part of the dipole–nucleus forward scattering amplitude $N(\vec{x}_\perp, \vec{b}_\perp, Y)$. In Sec. 4.2 we constructed such an amplitude in the Glauber–Gribov–Mueller multiple rescattering approximation. The resulting forward amplitude has no energy dependence, as one can see from Eq. (4.49), and therefore cannot be a realistic description of the high energy asymptotics of dipole–nucleus scattering. At the same time, the approach of Sec. 4.2 is valid only when the small-x evolution emissions are not important, that is, only for $\alpha_s Y \ll 1$. At higher energies, corresponding to rapidities Y satisfying $\alpha_s Y \gtrsim 1$, small-x evolution becomes important and can no longer be neglected.

We see that we need to resum the LLA corrections to the dipole–nucleus scattering amplitude (4.49). As usual we are interested in quantum evolution corrections that resum the powers of $\alpha_s \ln 1/x \sim \alpha_s Y$.[7] Just as in Sec. 4.2 we will be working in the rest frame of the nucleus, but this time we choose to work in the light cone gauge of the projectile dipole, $A^+ = 0$, if it is moving in the light cone plus direction. One can show by explicit calculation that for the multiple rescatterings in Fig. 4.5 this gauge is equivalent to the covariant gauge ($\partial_\mu A^\mu = 0$, see Sec. 3.3.1); therefore, our discussion in Sec. 4.2 remains valid in this new gauge. As in Sec. 4.2 we will be working either in the nucleus rest frame or in the frame in which the dipole is moving in the light cone plus direction while the target nucleus is moving in the minus direction.

We need to identify radiative corrections that bring in powers of $\alpha_s Y$. As we saw in Sec. 4.2, multiple rescatterings bring in only powers of α_s not enhanced by factors of Y (but enhanced by powers of A; the resummation parameter was $\alpha_s^2 A^{1/3}$). Therefore, additional t-channel gluon exchanges with new nucleons would not generate any powers of Y but would bring in only extra factors of α_s. These are not the corrections we are trying to resum now. Other possible corrections in the light cone gauge of the projectile dipole are modifications of the dipole wave function. The incoming dipole may have some gluons (and "sea" quarks) present in its wave function. For instance, the dipole may emit a gluon before interacting with the target; then the whole system of quark, antiquark, and gluon would rescatter in the nucleus, as shown in the upper panel of Fig. 4.23. The dipole may emit two gluons, which would then interact with the nucleus, along with the original $q\bar{q}$ pair, as shown in the lower panel of Fig. 4.23. In principle there could be many extra gluon emissions, as well as the generation of extra $q\bar{q}$ pairs in the incoming dipole's wave function. As we will shortly see, these gluonic fluctuations from Fig. 4.23 actually do bring the factors of α_s enhanced by powers of rapidity Y, i.e., they do generate leading logarithmic

[7] Quantum evolution is defined as the variation of a physical quantity with Q^2 and/or x owing quantum variations.

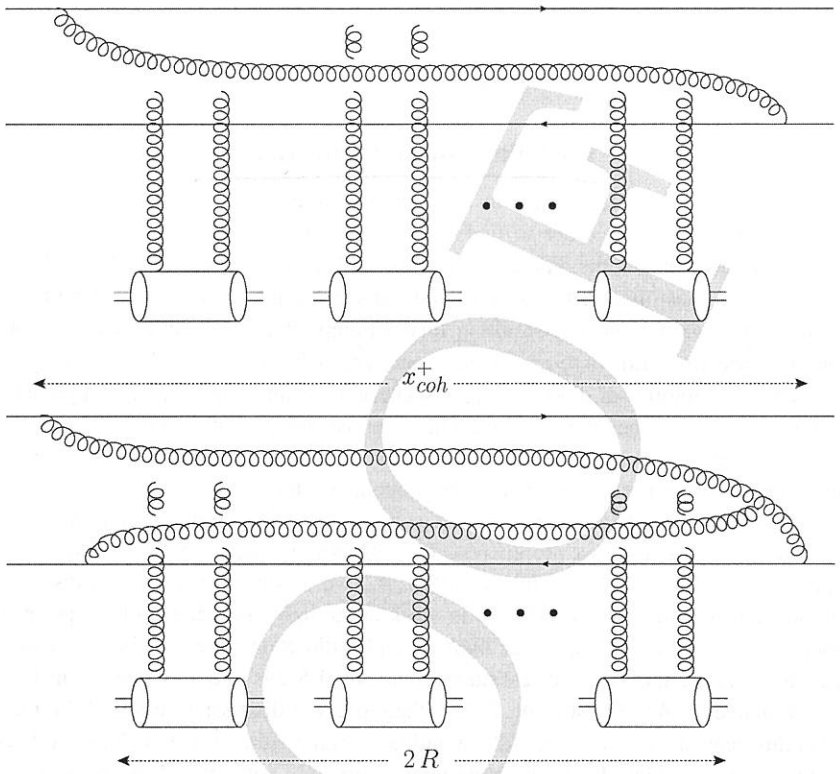

Fig. 4.23. Quantum evolution corrections to dipole–nucleus scattering due to one-gluon (upper panel) and two-gluon (lower panel) emissions. The lower panel also shows the coherence time scale for gluon emission x^+_{coh} and the nuclear size $2R$. At high energy $x^+_{coh} \gg 2R$: the figure does not fully reflect this scale difference.

corrections. Just as with the BFKL evolution, fluctuations leading to the formation of $q\bar{q}$ pairs actually enter at the subleading logarithmic level, bringing in powers of $\alpha_s^2 Y$, and are not important for the leading logarithmic approximation used in this chapter.

Several times above (see the discussion around Eqs. (2.156), (3.126), and (4.2)), we have used the fact that owing to the uncertainty principle, for an incoming dipole moving in the light cone plus direction a gluon with momentum k^μ in its wave function would have coherence length

$$x^+_{coh} \approx \frac{k^+}{k_\perp^2} \tag{4.129}$$

along the x^+-axis. Note straight away that t-channel gluon exchanges between the dipole and the nucleons in the nucleus, in the Glauber–Gribov–Mueller approximation of Sec. 4.2, have $k^+ = 0$ with eikonal accuracy (i.e., up to corrections suppressed by powers of the

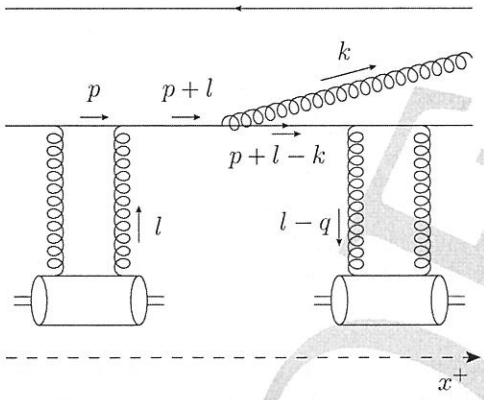

Fig. 4.24. A diagram with a gluon emission between the dipole interactions with two nucleons.

energy). Thus these t-channel gluons have $x^+_{coh} = 0$ and are instantaneous in the x^+ "time" direction in our eikonal picture. These are the instantaneous or Coulomb gluons. The instantaneous nature of these gluons explains why the dipole rescatters on the nucleons sequentially: as the nucleons are assumed to be separated in x^+, the dipole interacts with a nucleon as it crosses the latter's x^+-range, with interactions that are out of order, like that in Fig. 4.6B, not allowed by causality. The nucleons span the whole nucleus; thus the x^+-time interval filled with the instantaneous interactions of Fig. 4.5 is of the order of the nuclear radius R in the nuclear rest frame.

Consider now the gluon modifications to the incoming dipole's wave function shown in Fig. 4.23. If a gluon's k^+ is large enough, as is the case at high energy, the coherence lengths of these gluons would be much larger than the nuclear radius, $x^+_{coh} \gg R$, so that each gluon would coherently rescatter on the nucleons in the nucleus, just like the original dipole in Fig. 4.5. This is indeed what is shown in Fig. 4.23.

Note that gluons are emitted by the incoming dipole only before the multiple rescattering interaction (and absorbed back, after the interaction, into the forward amplitude). Emissions during the interaction are suppressed by the inverse powers of the center-of-mass energy of the scattering system. This can be checked via an explicit calculation in the covariant Feynman perturbation theory. Imagine a diagram with the gluon emitted or absorbed between the rescatterings, as shown in Fig. 4.24. As in our analysis of the graph in Fig. 4.9 above, we concentrate on the contribution of quark propagators to the l^--integral. We see that the diagram is proportional to

$$\int_{-\infty}^{\infty} \frac{dl^-}{2\pi} \frac{e^{-il^-\Delta x^+}}{[(p+l)^2 + i\epsilon][(p+l-k)^2 + i\epsilon]}$$
$$\approx \int_{-\infty}^{\infty} \frac{dl^-}{2\pi} \frac{e^{-il^-\Delta x^+}}{[p^+l^- - \perp^2 + i\epsilon][(p^+ - k^+)(k^- + l^-) - \perp'^2 + i\epsilon]} \tag{4.130}$$

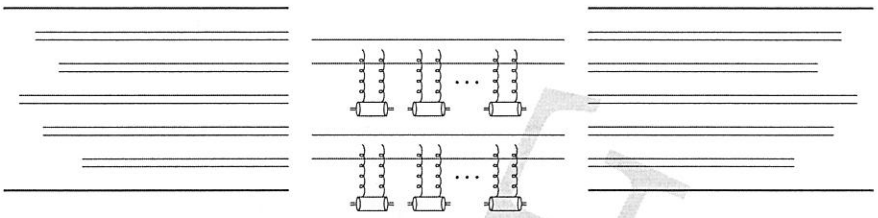

Fig. 4.25. Forward amplitude for dipole–nucleus scattering including small-x evolution: the incoming dipole develops a cascade of daughter dipoles, each of which interacts with the nucleus independently.

where $\perp$ and $\perp'$ denote the appropriate transverse momenta, whose exact values are not important to us here. We have used the fact that $l^+ = 0$ and assumed for simplicity that $p^- = 0$. We also changed the frame to that where the nucleus is moving along the negative light cone. Closing the integration contour in the lower half-plane we obtain

$$\frac{-i}{p^+(p^+ - k^+)} \frac{1}{k^- + \frac{\perp^2}{p^+} - \frac{\perp'^2}{p^+ - k^+}} \left[e^{-i \frac{\perp^2}{p^+} \Delta x^+} - e^{-i \left(-k^- + \frac{\perp'^2}{p^+ - k^+} \right) \Delta x^+} \right]$$

$$\approx \frac{-i}{p^{+2} k^-} \left(1 - e^{i k^- \Delta x^+} \right) \sim \frac{-1}{p^{+2} p'^-} = \frac{-1}{p^+ s}, \tag{4.131}$$

where we have used the fact that $p^+ \gg k^+$ and, more importantly, $\Delta x^+ \sim 1/p'^-$ with p'^- the large light cone momentum of a nucleon in the nucleus (such that $s = p^+ p'^-$ is the dipole–nucleon center-of-mass energy). This allowed us to expand the exponential in the second line of Eq. (4.131). Comparing with the rescatterings without gluon emission given in Eq. (4.37) (identifying k^+ in (4.37) with p^+ here), we see that gluon emission between rescatterings brings in suppression by a power of the energy s and can thus be neglected.

Alternatively we can consider this calculation in light cone perturbation theory. In this case, the emission of a gluon is allowed and is equally probable at any point throughout the coherence length of the parent dipole $x_{coh}^{q\bar{q}+} = p^+/p_\perp^2$, with p the momentum of the dipole and p^+ very large. The probability of emission of a gluon inside the nucleus (in the nuclear rest frame) is then proportional to $R/x_{coh}^{q\bar{q}+} \sim 1/p^+ \sim 1/s$; i.e., again, just as in Eq. (4.131) it is suppressed by a power of the center-of-mass energy s compared with emission outside the nucleus and can be neglected in the eikonal approximation considered here.

Our goal, therefore, is to resum the cascade of long-lived gluons that the dipole in Fig. 4.23 develops before interacting with the nucleus and then to convolute this cascade with the interaction amplitudes of the gluons with the nucleus. To resum the cascade we will assume the large-N_c limit and use Mueller's dipole model, presented in Sec. 4.3. In the large-N_c limit the gluon cascade translates into a dipole cascade, examples of which are shown in Figs. 4.19 and 4.22. As we have seen above, in the LLA gluon emissions do not change the transverse coordinates of the quark and antiquark lines in the parent dipole. Therefore, the color dipoles have the same transverse coordinates throughout the whole process: once they are created their transverse coordinates do not change. Resummation of the dipole cascade reduces to the set of diagrams represented in Fig. 4.25, which is

P1: SFK Trim: 247mm × 174mm Top: 13.707mm Gutter: 18.98mm
CUUK1947-04 CUUK1947/Kovchegov 978 0 521 11257 4 March 23, 2012 20:28

a generalization of Fig. 4.5 to the case of quantum evolution corrections. The incoming dipole develops a cascade of daughter dipoles through evolution according to Mueller dipole model.

The evolved system of dipoles interacts with the nucleus. The interaction is brief and does not change the transverse coordinates of the dipoles. In the large-N_c limit no dipole interacts with any other dipole during the evolution that generates all the dipoles. For a large nucleus the daughter dipole–nucleus interaction was calculated above in the GGM approximation and is given by Eq. (4.51). That result resums powers of $\alpha_s^2 A^{1/3}$. Analyzing the diagrams for the interaction of several dipoles with the nucleus we see that the GGM interaction of, say, two dipoles with a single nucleon is suppressed by extra powers of α_s not enhanced by $A^{1/3}$ and is therefore subleading and can be neglected. The interaction of two dipoles with two nucleons in the large-N_c limit is dominated by diagrams where each dipole interacts with only one nucleon (assuming both dipoles interact). In general one can argue that, in the large-N_c limit and at the leading order in A (or, equivalently, resumming powers of $\alpha_s^2 A^{1/3}$), the interaction of any number of dipoles with the nucleus is dominated by the *independent* interactions of each dipole with a different set of nucleons in the nucleus through multiple rescatterings of the type in Fig. 4.5. This is depicted in Fig. 4.25: there each dipole present in the dipole wave function may have interacted, by the time it hits the nucleus, with different nucleons in the nucleus by exchanging pairs of gluons. (It can be shown that only some dipoles thus interact.) Therefore, the dipoles are completely mutually noninteracting: they do not exchange gluons in the process of evolution, since those corrections would be suppressed by powers of N_c, and they interact with *different* nucleons in the nucleus; the last statement is correct at leading order in A (Kovchegov 1999).

Summation of the dipole cascade of Fig. 4.25 now becomes straightforward. Instead of calculating the forward dipole–nucleus scattering amplitude $N(\vec{x}_\perp, \vec{b}_\perp, Y)$ we start with the S-matrix $S(\vec{x}_\perp, \vec{b}_\perp, Y)$, which is related to N via Eq. (4.38). We write it here again for completeness:

$$S(\vec{x}_\perp, \vec{b}_\perp, Y) = 1 - N(\vec{x}_\perp, \vec{b}_\perp, Y). \tag{4.132}$$

As follows from the above discussion, $S(\vec{x}_{10}, \vec{b}_{0\perp}, Y)$ can be written as a convolution of the dipole cascade and the dipole interactions with the target, as shown in Fig. 4.25. Namely, it is a sum of the probability of finding one daughter dipole in the parent dipole, convoluted with the S-matrix for dipole–nucleus scattering in the GGM approximation, and the probability of finding two dipoles, convoluted with their multiple rescattering interactions with the nucleus, etc. We write (Kovchegov 1999)

$$S(\vec{x}_{10}, \vec{b}_\perp, Y) = \sum_{k=1}^{\infty} \frac{1}{k!} \int d^2 r_1 d^2 b_1 \cdots d^2 r_k d^2 b_k \times \frac{\delta^k Z(\vec{x}_{10}, \vec{b}_\perp, Y; u)}{\delta u(\vec{r}_{1\perp}, \vec{b}_{1\perp}) \cdots \delta u(\vec{r}_{k\perp}, \vec{b}_{k\perp})}\bigg|_{u=0} s_0(\vec{r}_{1\perp}, \vec{b}_{1\perp}) \cdots s_0(\vec{r}_{k\perp}, \vec{b}_{k\perp}). \tag{4.133}$$

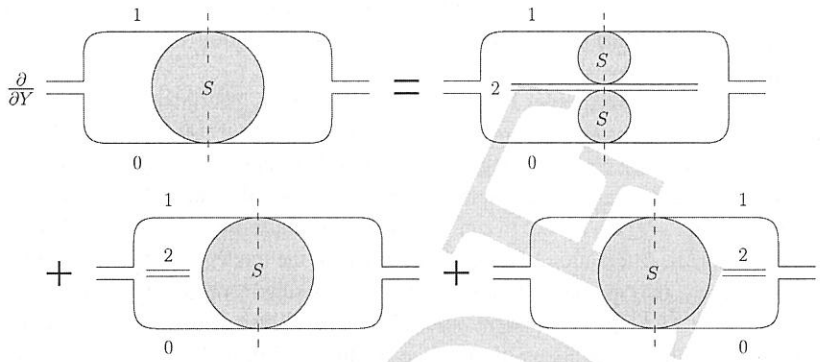

Fig. 4.26. Diagrammatic representation for the evolution equation of the S-matrix for dipole–nucleus scattering, denoted by a shaded circle. The vertical broken lines denote the interaction with the target.

Here

$$\left.\frac{\delta^k Z(\vec{x}_{10}, \vec{b}_\perp, Y; u)}{\delta u(\vec{r}_{1\perp}, \vec{b}_{1\perp}) \cdots \delta u(\vec{r}_{k\perp}, \vec{b}_{k\perp})}\right|_{u=0} \tag{4.134}$$

gives the probability of finding *exactly* k daughter dipoles in the parent dipole wave function (cf. Eq. (4.71)), and

$$s_0(\vec{r}_\perp, \vec{b}_\perp) \equiv S(\vec{r}_\perp, \vec{b}_\perp, Y = 0) = \exp\left\{-\frac{x_\perp^2 Q_{s0}^2(\vec{b}_\perp)}{4} \ln \frac{1}{x_\perp \Lambda}\right\}, \tag{4.135}$$

as follows from Eqs. (4.51) and (4.132).

Summing the series in Eq. (4.133) yields (see Eq. (4.70))

$$S(\vec{x}_{10}, \vec{b}_\perp, Y) = Z\left(\vec{x}_{10}, \vec{b}_\perp, Y; u = s_0\right) \tag{4.136}$$

(Kovchegov 1999). This relation shows that both the dipole–nucleus S-matrix and the generating functional Z obey the same nonlinear evolution equation. The initial condition for Z in (4.76) is replaced by Eq. (4.135).

We see that the evolution of $S(\vec{x}_\perp, \vec{b}_\perp, Y)$ is the same as the evolution of the generation functional Z in Sec. 4.3: it is illustrated in Fig. 4.26 (cf. Fig. 4.21). The dipole cascade and its interaction with the target are denoted by a shaded circle. In one step of the evolution in energy (or rapidity) a soft gluon is emitted in the dipole. If the gluon is real then the original dipole is split into two dipoles, as shown at top right of Fig. 4.26; these dipoles proceed to evolve and interact (or not) independently with the target (the S-matrix includes the noninteraction term, the "1" in Eq. (4.132)). Virtual corrections, given by the two lower diagrams in Fig. 4.26, lead only to the parent dipole's subsequent evolution and interaction with the target. We obtain an evolution equation for the S-matrix (Balitsky 1996, Kovchegov

P1: SFK Trim: 247mm × 174mm Top: 13.707mm Gutter: 18.98mm
CUUK1947-04 CUUK1947/Kovchegov 978 0 521 11257 4 March 23, 2012 20:28

1999):

$$\frac{\partial}{\partial Y} S(\vec{x}_{10}, \vec{b}_\perp, Y) = \frac{\alpha_s N_c}{2\pi^2} \int d^2x_2 \frac{x_{10}^2}{x_{20}^2 x_{21}^2} \times \left[S\left(\vec{x}_{12}, \vec{b}_\perp + \frac{\vec{x}_{20}}{2}, Y\right) S\left(\vec{x}_{20}, \vec{b}_\perp + \frac{\vec{x}_{21}}{2}, Y\right) - S(\vec{x}_{10}, \vec{b}_\perp, Y) \right]. \quad (4.137)$$

The initial condition for this evolution equation is given by $S(\vec{x}_{10}, \vec{b}_\perp, Y = 0)$ in Eq. (4.135). As usual $\vec{b}_\perp = (\vec{x}_{1\perp} + \vec{x}_{0\perp})/2$.

Using Eq. (4.132) in Eq. (4.137) we derive an evolution equation for the imaginary part of the forward dipole–nucleus scattering amplitude N (Balitsky 1996, Kovchegov 1999):

$$\frac{\partial}{\partial Y} N(\vec{x}_{10}, \vec{b}_\perp, Y) = \frac{\alpha_s N_c}{2\pi^2} \int d^2x_2 \frac{x_{10}^2}{x_{20}^2 x_{21}^2} \times \left[N\left(\vec{x}_{12}, \vec{b}_\perp + \frac{\vec{x}_{20}}{2}, Y\right) + N\left(\vec{x}_{20}, \vec{b}_\perp + \frac{\vec{x}_{21}}{2}, Y\right) - N(\vec{x}_{10}, \vec{b}_\perp, Y) - N\left(\vec{x}_{12}, \vec{b}_\perp + \frac{\vec{x}_{20}}{2}, Y\right) N\left(\vec{x}_{20}, \vec{b}_\perp + \frac{\vec{x}_{21}}{2}, Y\right) \right]. \quad (4.138)$$

This is the Balitsky–Kovchegov (BK) evolution equation. The initial condition for the BK evolution is given by Eq. (4.51):

$$N(\vec{x}_\perp, \vec{b}_\perp, Y = 0) = 1 - \exp\left\{ -\frac{x_\perp^2 Q_{s0}^2(\vec{b}_\perp)}{4} \ln \frac{1}{x_\perp \Lambda} \right\}, \quad (4.139)$$

where we have replaced $Q_s^2(\vec{b}_\perp)$ from Eq. (4.51) by $Q_{s0}^2(\vec{b}_\perp)$ to underscore that this is the saturation scale in the initial condition for the evolution. (As we will see shortly, the saturation scale is modified by the nonlinear BK evolution equation: in particular it becomes dependent on the rapidity Y.) Equation (4.138) resums all powers of the multiple rescattering parameter $\alpha_s^2 A^{1/3}$, along with the leading logarithms of energy in the large-N_c limit given by powers of $\alpha_s N_c Y$.

Below we will sometimes use a more compact notation for the dipole–nucleus amplitude,

$$N(\vec{x}_{1\perp}, \vec{x}_{0\perp}, Y) \equiv N(\vec{x}_{10}, \vec{b}_\perp, Y). \quad (4.140)$$

Using this notation, we can rewrite Eq. (4.138) as

$$\frac{\partial}{\partial Y} N(\vec{x}_{1\perp}, \vec{x}_{0\perp}, Y) = \frac{\alpha_s N_c}{2\pi^2} \int d^2x_2 \frac{x_{10}^2}{x_{20}^2 x_{21}^2} \times \left[N(\vec{x}_{1\perp}, \vec{x}_{2\perp}, Y) + N(\vec{x}_{2\perp}, \vec{x}_{0\perp}, Y) - N(\vec{x}_{1\perp}, \vec{x}_{0\perp}, Y) - N(\vec{x}_{1\perp}, \vec{x}_{2\perp}, Y) N(\vec{x}_{2\perp}, \vec{x}_{0\perp}, Y) \right]. \quad (4.141)$$

P1: SFK Trim: 247mm × 174mm Top: 13.707mm Gutter: 18.98mm
CUUK1947-04 CUUK1947/Kovchegov 978 0 521 11257 4 March 23, 2012 20:28

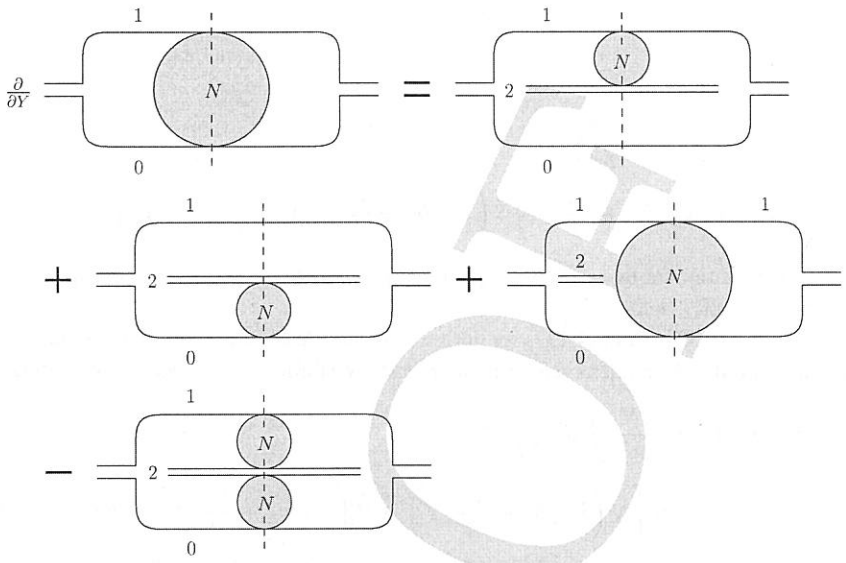

Fig. 4.27. Diagrammatic representation of the BK evolution equation for the forward dipole–nucleus scattering amplitude N, denoted by a shaded circle. Only one virtual term is shown, for brevity.

The BK equation is represented diagrammatically in Fig. 4.27. Balitsky–Kovchegov evolution has a simple physical meaning. At fixed rapidity a colorless dipole with size x_{10} decays into two dipoles with sizes x_{12} and x_{20}. Either one dipole proceeds to evolve and interact with the target while the other dipole remains a spectator (the first two, linear, terms after the equals sign in Fig. 4.27) or both dipoles evolve and interact with the target (the nonlinear term in Fig. 4.27). The minus sign in front of the nonlinear term reflects the fact that taking into account two independent interactions overestimates the result. The nonlinear term corresponds to the shadowing corrections in the GGM approach: for instance, expanding Eq. (4.45) in powers of interactions with the nucleons we see that the quadratic term enters with a minus sign. The reason for that minus sign is the same as the reason for the minus sign in the last term of Eq. (4.138).

Equation (4.138) was originally derived by Balitsky (1996) in the framework of the effective theory of high energy interactions and, independently, by one of the present authors (Kovchegov 1999) using the formalism of Mueller's dipole model (Mueller 1994, 1995). It was rederived by Braun (2000a) using the large-N_c limit of the expression for the triple pomeron vertex from Bartels and Wusthoff (1995) in a resummation of the fan diagrams in Fig. 3.23.

Comparing the linear part of the BK equation (the first three terms on the right of Eq. (4.138)) with Eq. (4.87), we see that the linear terms in the BK equation give the coordinate-space BFKL equation. As already mentioned, the nonlinear term can be obtained

from the triple-pomeron vertex in the large-N_c limit (Braun 2000a). Hence Eq. (4.138) has the overall structure of the GLR equation and corresponds to fan diagram resummation in the conventional Feynman perturbation theory. It is natural to expect that the BK evolution leads to the same physical effects as the GLR equation: for a given fixed dipole size, the dipole amplitude N would start out growing with rapidity owing to BFKL evolution (see Eq. (4.102)); the nonlinear term would become important at higher rapidity and lead to saturation and slowdown of the energy growth. In the next section we will see that this is indeed the case.

In solving the BK equation (4.138) one often (but not always) assumes that the variation in the amplitude $N(\vec{x}_{10}, \vec{b}_\perp, Y)$ with the impact parameter $\vec{b}_\perp$ is small when $\vec{b}_\perp$ varies over distance scales comparable with the dipole size $|\vec{x}_{10}|$. This is indeed true for scattering on a very large nucleus far away from its edges. This assumption allows to neglect the shifts in the impact parameter on the right-hand side of Eq. (4.138). Moreover, assuming that the nucleus is isotropic we may neglect the angular dependence of $\vec{x}_{10}$. We thus may replace $N(\vec{x}_{10}, \vec{b}_\perp, Y)$ approximately by $N(x_{10}, Y)$ in Eq. (4.138), obtaining

$$\frac{\partial}{\partial Y} N(x_{10}, Y) = \frac{\alpha_s N_c}{2\pi^2} \int d^2x_2 \frac{x_{10}^2}{x_{20}^2 x_{21}^2} \times \Big[N(x_{12}, Y) + N(x_{20}, Y) - N(x_{10}, Y) - N(x_{12}, Y)\, N(x_{20}, Y) \Big]. \tag{4.142}$$

Performing the Fourier transformation

$$N(x_\perp, Y) = x_\perp^2 \int \frac{d^2k}{2\pi} e^{i\vec{k}_\perp \cdot \vec{x}_\perp} \tilde{N}(k_\perp, Y), \tag{4.143}$$

we write (Kovchegov 2000)

$$\frac{\partial \tilde{N}(k_\perp, Y)}{\partial Y} = \bar{\alpha}_s \chi \left[0, \frac{i}{2} \left(1 + \frac{\partial}{\partial \ln k_\perp} \right) \right] \tilde{N}(k_\perp, Y) - \bar{\alpha}_s \tilde{N}^2(k_\perp, Y). \tag{4.144}$$

This equation is useful for obtaining approximate solutions for the BK evolution that we will present below. Also, note that making the identification

$$\phi(x, k_\perp^2) = \frac{N_c S_\perp}{\alpha_s \pi^2} \tilde{N}(k_\perp, Y = \ln 1/x) \tag{4.145}$$

in Eq. (4.144) reduces it to the GLR equation (3.128). This is indeed remarkable: however, there exists no physical justification for the Fourier transformation (4.143). At the lowest, two-gluon-exchange, order the relation between the dipole amplitude N and the unintegrated gluon distribution ϕ should be of the form of Eq. (4.98) (with f there proportional to ϕ). In the region where multiple rescatterings and quantum evolution are important, the exact relation between N and ϕ is not clear.